THE JOURNAL OF PHYSICAL CHEMISTRY B

Article

pubs.acs.org/JPCB

Nanocomposites of Polystyrene-*b*-Poly(isoprene)-*b*-Polystyrene Triblock Copolymer with Clay–Carbon Nanotube Hybrid Nanoadditives

Apostolos Enotiadis,[†] Kiriaki Litina,[†] Dimitrios Gournis,*[,†] Sofia Rangou,[†,‡] Apostolos Avgeropoulos,*[,†] Panagiotis Xidas,[§] and Kostas Triantafyllidis*[,§]

[†]Department of Materials Science Engineering, University of Ioannina, 45110 Ioannina, Greece

[‡]Institute of Polymer Research, Helmholtz-Zentrum Geesthacht, Max-Planck-Str. 1, 21502, Geesthacht, Germany

[§]Department of Chemistry, Aristotle University of Thessaloniki, 54124 Thessaloniki, Greece

Supporting Information

ABSTRACT: Polystyrene-*b*-polyisoprene-*b*-polystyrene (PS-*b*-PI-*b*-PS), a widely used linear triblock copolymer of the glassy-rubbery-glassy type, was prepared in this study by anionic polymerization and was further used for the development of novel polymer nanocomposite materials. Hybrid nanoadditives were prepared by the catalytic chemical vapor deposition (CCVD) method through which carbon nanotubes were grown on the surface of smectite clay nanolayers. Sidewall chemical organo-functionalization of the nanotubes was performed in order to enhance the chemical compatibilization of the clay–CNT hybrid nanoadditives with the hydrophobic triblock copolymer. The hybrid clay–CNT nanoadditives were incorporated in the copolymer matrix by a simple solution-precipitation method at two nanoadditive to polymer loadings (one low, i.e., 1 wt %, and one high, i.e., 5 wt %). The resulting nanocomposites were characterized by a combination of techniques and compared with more classical nanocomposites prepared using organo-modified clays as nanoadditives. FT-IR and Raman spectroscopies verified the presence of the hybrid nanoadditives in the final nanocomposites, while X-ray diffraction and transmission electron microscopy proved the formation of fully exfoliated structures. Viscometry measurements were further used to show the successful incorporation and homogeneous dispersion of the hybrid nanoadditives in the polymer mass. The so prepared nanocomposites exhibited enhanced mechanical properties compared to the pristine polymer and the nanocomposites prepared by conventional organo-clays. Both tensile stress and strain at break were improved probably due to better interfacial adhesion of the clay–CNT hybrid of the flexible rubbery PI middle blocks of the triblock copolymer matrix.

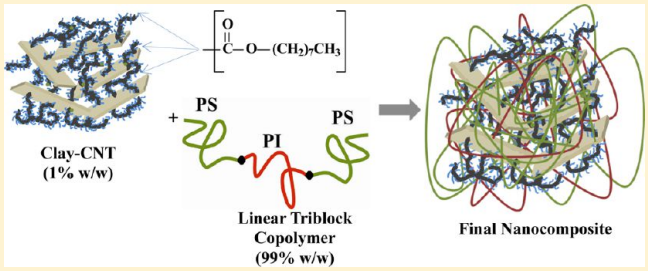

1. INTRODUCTION

Block copolymers have shown a great impact in the evolution of polymer science and macromolecular engineering in the past decades.[1] Their interesting properties derive from their ability to self-assemble and form unique and well-defined periodic nanostructures.[2] Incompatible blocks such as polystyrene (PS) and poly(isoprene) (PI) self-organize in the bulk, and depending on their length, the sequence of the monomers, and the final macromolecular architecture, they form periodic and ordered nanostructures. What has been of great importance, especially in the case of PS-*b*-PI-*b*-PS (or SIS) linear triblock copolymers, is the wide range of potential applications that have been reported based especially on the mechanical properties of the proposed material, since it behaves as a thermoplastic elastomer. Triblock copolymers of the glassy-rubbery-glassy type with increased rubbery composition (as in our case, ~38%) make mechanically useful elastomers, as both ends of the rubbery midblock are held fixed by the glassy phases. These copolymers can be considered as physically cross-linked ordered systems which can be processed at high temperatures, having also high melting points, and can be recyclable. Since the polystyrene (PS) and the polydiene microdomains still retain some characteristics of their respective homopolymers, such materials exhibit unique properties. In particular, they exhibit two glass transition temperatures, characteristic of the two types of microdomains involved in the linear architecture. The mechanical behavior of such elastomeric triblocks exhibiting the usual microdomain morphologies has been investigated extensively.[3] Styrenic thermoplastic elastomers (TPEs) are the most studied, since they are well-defined materials and exhibit in most cases low molecular weight polydispersity. The mechanical properties of TPEs depend on their morphology and in stress–strain testing and for up to 100% strain of polygranular isotropic PS-*b*-PI-*b*-PS triblock copolymers with different morphologies, the sample with the double gyroid (DG) morphology exhibits a stable

Received: September 20, 2012
Revised: December 8, 2012
Published: December 20, 2012

neck, whereas the samples with spherical, cylindrical and lamellar morphology do not exhibit necking.[4] In addition, the yield stress of the DG is much higher than that of the sample with cylindrical morphology. There is a major drawback in using triblock copolymers with DG structures due to the low volume fraction regime that appears (0.27−0.34);[5] therefore, mostly cylindrical adopted structures have been studied and applied commercially and such a structure is being adopted for further investigation in the present work.

Attention in polymer research the last two decades has also been focused on the development of novel nanocomposites in order to enhance several properties of neat polymeric matrixes using molecular or nanoscale reinforcements. In most cases, the matrix of the polymer is filled with several synthetic and/or natural compounds in order to increase properties such as tensile strength, modulus, heat resistance and stability, electrical conductivity, and barrier properties.[6] A homogeneous dispersion of the nanoadditives and utilization of their high available surface area (per unit mass) for interaction with the polymer are the key objectives for the preparation of polymer nanocomposites with improved properties. Many different types of inorganic nanostructures have been studied as polymer nanoadditives including one-dimensional materials, like carbon nanotubes or nanofibers, two-dimensional such as layered silicate minerals (clays), LDHs, or graphene, and three-dimensional such as inorganic particles (silica or carbon nanoparticles).[7]

Over the last decades, many efforts have been made for the development of polymer nanocomposites using swellable clays as nanoadditives.[6a,8] The presence of two-dimensional platelike silicate layers in the polymer matrix induces significant gains in thermal stability,[9] mechanical,[10] and barrier[11] properties of the resulting nanocomposites. Depending on the degree of clay nanolayer dispersion within the polymer matrix, it is possible to synthesize three different kinds of composites: (1) conventional composites, where the organic component is not inserted between the nanolayers of the clay which keep their original stacking, thus creating a conventional phase-separated composite and the only possible reinforcement can derive from the clay microparticles (microcomposite), (2) intercalated nanocomposites, where the polymer chains are intercalated between the clay nanolayers while keeping a relatively ordered stacking but with increased intragallery space, (3) the exfoliated state in which larger amounts of polymer are inserted within the nanolayers that induce a random dispersion of the individual nanolayers within the bulk polymer phase.[6b] The preparation procedures of these nanocomposites include solution, melt intercalation, and in situ polymerization.[6b,12] Solution intercalation has been very effective in incorporating exfoliated clays into polymers.[13]

In addition to layered silicates, single and multiwall carbon nanotubes (CNTs) have been also studied quite extensively as polymer nanoreinforcing agents. Since their discovery,[14] CNTs have attracted unlimited attention due to their unique properties such as huge mechanical strength and high electrical and thermal conductivity.[15] The most common synthetic method is based on chemical vapor deposition; however, this method in most cases leads to the formation of some defects on CNTs which may affect their physical and chemical properties. Although the CNTs can induce a combination of exceptional functional properties in the resulting nanocomposite,[16] the main drawback is the difficulty of dispersing the individual nanotubes homogeneously within the polymer matrix in order to form a continuous network which maximizes the resulting effects. CNTs are insoluble in common solvents and polymers and they easy agglomerate (bundle together), thus leading to many defects in the final nanocomposites.[17] Side wall chemical organo-functionalization is one of the most effective techniques to achieve the homogeneous dispersion of CNTs in the polymer, since their surface develops a more organophilic nature and strong interface adhesion can be achieved between the functionalized carbon nanotubes and the surrounding polymer chains.[18]

Hybrid nanostructured materials, in which carbon nanotubes are rooted on the surface of smectite clay nanolayers,[19] are particularly attractive for polymer reinforcement applications, since the combined benefits from the two-dimensional smectite clays and the one-dimensional carbon nanotubes can provide outstanding functionalities and properties to the resulting nanocomposite materials. Zhang et al.[20] demonstrated that the incorporation of CNT/clay hybrid systems into nylon-6 by simple melt blending led to exfoliated nanocomposites with impressive mechanical properties. Compared to the corresponding neat polymer, the tensile modulus and the tensile strength of the nanocomposite were greatly improved, approximately 290 and 150%, respectively, by incorporating only 1 wt % CNT/clay hybrid reinforcement. In addition, Li and co-workers[21] showed that reinforcement of poly(vinyl alcohol) with the hybrid clay−CNT additive resulted in novel nanocomposites with improved thermal and dynamic mechanical properties compared to the starting polymer. The same group[22] created nanocomposites of epoxy resins using the same hybrid nanoadditive which showed a dramatic improvement in the mechanical properties of the pristine epoxy resin. More specifically, the Vicker's hardness and impact strength of the final nanocomposite (by incorporating only 1 wt % CNTs/clay) were improved by 36 and 110%, respectively.

The same hybrid nanoadditive can be used for the reinforcement not only of homopolymers but also of diblock copolymers. As we showed recently,[23] nanocomposites of polystyrene-*b*-polyisoprene diblock copolymer with carbon nanotubes rooted on layered silicates could be successfully prepared by a solution-precipitation method. Finally, Jehng and co-workers[24] demonstrated the construction of high-sensitivity H_2O_2 sensors by incorporating a three-dimensional clay−CNT network in Nafion polymer membranes. The sensitivity for H_2O_2 detection was increased dramatically after the insertion of the hybrid nanoadditive due to the electro-conductivity of CNTs.

In the present study, novel nanocomposites of polystyrene-*b*-polyisoprene-*b*-polystyrene triblock copolymer (PS-*b*-PI-*b*-PS) with carbon nanotubes rooted on smectite clay nanolayers (hybrid clay−CNT nanoadditives) were developed. The triblock copolymer used in this work was chosen to be of the PS-*b*-PI-*b*-PS type, since such materials have been extensively studied and their molecular and morphological behavior is well-known and handled.[5,25] Nanocomposites of the triblock copolymer with the hybrid clay−CNTs were prepared by a solution-precipitation method at two nanoadditive to polymer loadings (1 and 5 wt %) and were compared with nanocomposites prepared—at the same conditions and loadings—using classical organo-modified clays as nanoadditives. The resulting nanocomposites were characterized by a combination of X-ray diffraction, FT-IR and Raman spectroscopies, thermal analysis, viscometry measurements, size exclusion chromatog-

raphy, transmission electron microscopy, and tensile properties measurements.

2. EXPERIMENTAL SECTION

2.1. Synthesis of PS-*b*-PI-*b*-PS Triblock Copolymer. The triblock copolymer was prepared by anionic polymerization using high-vacuum techniques in evacuated, *n*-BuLi-washed, benzene-rinsed glass vessels. The purification of monomers: styrene (Merck), isoprene (Fluka), and the solvents: benzene, tetrahydrofuran (Merck) to the standards required for anionic polymerization have been described elsewhere.[26] Additions were made through break-seals, and aliquot removals were accomplished through heat sealing of the proper constrictions. *sec*-BuLi (Aldrich) was used as received by diluting the appropriate amount (1.4 M in cyclohexane) in a custom-made glass apparatus with benzene to the required concentration.

2.2. Organic Modified Clay (C_{16}−SWy). The clay used in this work was a natural Wyoming montmorillonite (SWy-2) obtained from the Source Clay Minerals Repository, University of Missouri, Columbia, with a cation-exchange capacity (CEC) of 76.4 mequiv/100 g of clay. The clay was fractionated to <2 μm by gravity sedimentation and purified by standard methods.[27] Sodium-exchanged samples were prepared by immersing the clay into a 1 N solution of sodium chloride. Cation exchange was complete by washing and centrifuging four times with a dilute solution of NaCl. The samples were finally washed with distilled−deionized water, transferred into dialysis tubes in order to obtain chloride free clays, and then dried at room temperature.

To prepare a classical organo-clay, a solution of the surfactant (hexadecyltrimethyl ammonium bromide) in water (1.5 times the CEC of the clay) was added slowly to an aqueous 1 wt % clay suspension under vigorous stirring. The mixture was stirred for 24 h, centrifuged, washed with water three times, and air-dried by spreading on a glass plate.

2.3. Clay−Carbon Nanotube Hybrids (SWy−CNT). A montmorillonite clay suspension in water (1 wt %) was reacted with aliquots of a $NiCl_2{\cdot}6H_2O$ aqueous solution (1 N) such that the amount of the nickel cations added corresponds to 5 times the CEC of the clay. The solution was stirred for 3 h, and then, the Ni-exchanged clay was separated by centrifugation and was rinsed repeatedly with distilled−deionized water. It was then dried at room temperature and finally calcined at 450 °C for 4.5 h. Carbon nanotubes were synthesized by catalytic decomposition of acetylene over the Ni-clay catalyst in a fixed bed flow reactor at 700 °C.[19,28] About 100 mg of the catalyst was placed in an alumina boat which was placed in a tubular furnace with an inner diameter of 2.2 cm and length of 90 cm. The catalyst was heated up to 700 °C under an argon (Ar) atmosphere and was then reacted with acetylene at the same temperature for 40 min using a feed flow of argon/acetylene mixture (10 and 90 cm^3/min, respectively). The catalyst was then cooled down to room temperature under pure argon and the formed clay−CNT composite material was collected from the ceramic boat.

The produced carbon nanotubes developed on the clay surfaces were organo-functionalized as follows: 600 mg of the clay/CNT hybrid material was suspended in 80 mL of concentrated sulfuric acid/nitric acid mixture (3:1 (v/v)) and sonicated for 3 h. The suspension was then centrifuged and washed six times with water, in order to remove the excess of sulfuric and nitric acid, and dried at 50 °C in a vacuum overnight. 60 mg of the hybrid material bearing the purified/carboxylated nanotubes was sonicated in 90 mL of an aqueous NaOH solution (10 mM) for 2 min in order to produce the sodium salt of the carboxylated nanotubes. 100 mg of tetra-*n*-octylammonium bromide (TOAB) and 1.5 mL of hexadecyl-bromide were then added to the black homogeneous suspension, and the mixture was refluxed at 80 °C for 4 h under vigorous stirring.[18a] The solid precipitate was collected, resuspended in $CHCl_3$, centrifuged, washed with ethanol, and dried at 50 °C in a vacuum overnight.[23]

2.4. Preparation of the Nanocomposites. Triblock copolymer nanocomposites containing 1 and 5 wt % nano-additives (organoclay or clay−CNT) were prepared as follows: an appropriate amount of the triblock copolymer was diluted in toluene (10 mL), and the solution was reacted with aliquots of the corresponding filler suspension in toluene as well (5 mL). The mixture was then stirred for 3 h, precipitated with methanol, and air-dried by being spread on glass plates. Finally, the solid samples were heated for 2 h under a vacuum at 140 °C for the efficient removal of the solvent. The latter was controlled with DSC measurements (not shown here).

2.5. Characterization of materials. Size exclusion chromatography (SEC) experiments were carried out at 30 °C using a Spectra System PL 1000 pump, a Shodex RI 101 refractive index detector, and a Spectra System UV-1000 detector. Three Mixed-C (Polymer Laboratories, with porous for efficient separation of molecules varying from 2000 to 4×10^6 g/mol) columns were used, thermostated in a Lab Alliance column oven at 30 °C. THF, distilled over CaH_2 and sodium, was the carrier solvent at a flow rate of 1 mL/min. Proton nuclear magnetic resonance spectroscopy (^{1}H NMR) was used for the determination of the composition and the microstructure of the PI chains (~90% 1,4-microstructure and ~10% 3,4- and 1,2-microstructure, respectively). The experiments were carried out in $CDCl_3$ at 30 °C using a Bruker AVANCE II spectrometer. Data were processed using UXNMR (Bruker) software. The X-ray powder diffraction data were collected on a D8 Advanced Bruker diffractometer by using Cu K_a (40 kV, 40 mA) radiation and a secondary beam graphite monochromator. The patterns were recorded in a 2-theta range from 2 to 30°, in steps of 0.02° and counting time 2 s per step. FTIR spectra were measured with a Perkin-Elmer Spectrum GX infrared spectrometer, in the region 400−2000 cm^{-1}, equipped with a DTGS detector. Each spectrum was the average of 32 scans collected at 2 cm^{-1} resolution. Samples were in the form of KBr pellets containing ca. 2 wt % clay or clay−CNT samples, while nanocomposites were measured as received. The viscometry measurements were conducted by using a type 0c Ubbelohde suspended level dilution viscometer (suitable only for toluene which is a nonselective solvent for both blocks) at a thermostated water bath of 35 °C. Toluene is a common good solvent for both segments of the copolymer. The solvent was refluxed over CaH_2 for 24 h and was fractionally distilled prior to use. Raman spectra over the range 1000−2000 cm^{-1} were recorded with a Renishaw RM 1000 Micro-Raman system using a Nd:YAG laser excitation line at 532 nm. A power of 0.5−1 mW and 1 μm focus spot were used in order to avoid photodecomposition of the samples.

Transmission electron microscopy (TEM) was employed for the morphological characterization of the nanocomposites. A 2% w/v solution of the nanocomposite mixture containing the prepolymer and the clay or clay−CNT nanoadditives was prepared in toluene. A drop of this solution was evaporated on

dx.doi.org/10.1021/jp309361b | J. Phys. Chem. B 2013, 117, 907−915

a 200 mesh carbon coated Cu grid creating a thin film of approximately 50 nm in thickness. The grids were subsequently annealed above the T_g value of the PS component for 7 days (at 130 °C) under a vacuum. A 2% w/v solution in water of osmium tetroxide (OsO_4) was used whenever appropriate as a staining agent for preferential staining of the PI component, which therefore appears black in the TEM images, whereas the PS segments appear white. Composites with organoclays were stained with OsO_4, while those with clay−CNTs were examined as received after the annealing in order to better distinguish the CNTs from the copolymer (which appears light to dark gray in the TEM images). TEM experiments were carried out on a JEOL 200CX instrument equipped with a postcolumn Gatan Imaging Filter (GIF) operated in 200 KeV on both stained and unstained films.

The tensile properties (stress and strain at break, elastic modulus) of the pristine polymer and the nanocomposites were measured on an Instron 3344 dynamometer, in accordance with the ASTM D638 method using a crosshead speed of 5 mm/min and dogbone-shaped specimens with dimensions of 30 mm long × 2 mm thick × 5 mm wide along the center of the casting (narrow region). The exact dimensions of each specimen were measured before the test. Three specimens from each nanocomposite sample were tested to establish reproducibility of the measurements.

3. RESULTS AND DISCUSSION

The triblock copolymer was synthesized via anionic polymerization techniques using sequential addition of the monomers in the solvent under high vacuum. The reactions that take place are presented in Scheme 1. More details on the synthesis

Scheme 1. Synthetic Pathway of the Triblock Copolymer

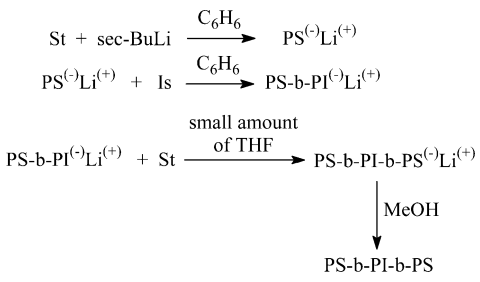

procedure are given in the Supporting Information (Figure S1 represents the successful synthesis of the copolymer through SEC, and Table S1 includes all the molecular characteristics from size exclusion chromatography and membrane osmometry).

For the synthesis of clay−CNT hybrid nanoadditives, montmorillonite clay was loaded with nickel cations that function as catalysts in the growth of carbon nanotubes via catalytic decomposition of acetylene.[19,28,29] In order to enhance the chemical compatibilization of the hybrid nanoadditives developed with the hydrophobic triblock copolymer, side-wall chemical organo-functionalization of the nanotubes was performed through covalent attachment of aliphatic groups on the surface of the nanotubes.[23] A full characterization (including powder XRD, Raman spectroscopy, thermal analysis, SEM and TEM) was performed, as we have reported elsewhere,[19,23,28,29] revealing the sample morphology, composition, and structure of the hybrid nanoadditives. High quality multiwall carbon nanotubes, with an average diameter between 20 and 35 nm and length up to several micrometers, are formed which are rooted on the clay layers forming a three-dimensional network while clay platelets are being in a delaminated state. In general, in the clay−CNT nanoadditive, the total mass of carbon nanotubes corresponds to approximately 30 wt %, while the amount of aliphatic ester groups bonded to the surfaces of CNTs is ∼10 wt % and the amount of the clay mineral in the hybrid filler is about 60 wt %.[23] Side-wall functionalization of CNTs provides stable dispersions of the clay−CNT hybrids in nonpolar solvents, such as toluene, allowing the fabrication of polymer composites by mixing the components in solution at room temperature. In fact, both hybrid nanoadditive and the triblock copolymer were diluted in toluene and the resulting dispersion was precipitated by methanol, leading to the formation of a homogeneous nanocomposite phase. A schematic illustration showing the procedure of growing CNTs on Ni-clay, the purification and chemical organo-functionalization step, and finally the incorporation of hybrid clay−CNT nanoadditives into the copolymer is presented in Scheme 2.

X-ray diffraction measurements provide a powerful tool to evaluate the degree of clay nanolayer dispersion within the polymer matrix and the type of nanocomposite phase created. The XRD patterns of the different clay variants and the triblock copolymer nanocomposites with the clay−CNT at different loadings (1 and 5 wt %) are shown in Figure 1. The diffraction pattern of Ni-montmorillonite heated at 450 °C in air (Figure 1a) shows a peak with a maximum at 2θ = 9.25° that corresponds to a d_{001}-spacing of 9.6 Å, which actually equals the thickness of the layer of 2:1 clay minerals;[30] the relatively low *d*-spacing of the calcined clay is due to the absence of water molecules between the nanolayers which increase the *d*-spacing to ca. 12.5 Å in the hydrated clay. The intensity of the 001 peak after the production of CNTs on the surface of clay layers (Figure 1b) is significantly lower, implying that the majority of the layers have lost their ordered stacking and exhibit an exfoliated structure. In the same pattern, the appearance of a new peak at 2θ = 26.4°, which corresponds to the 002 reflection of graphite structure, is also present, revealing the successful production of good quality CNTs.[31] The same peak is also observed in the pattern of the clay−CNT sample after the chemical organo-functionalization (Figure 1c). Moreover, the absence of the 001 diffraction peak (due to ordered stacking of clay layers) in the patterns of the final nanocomposites (Figure 1e and f) indicates the creation of fully exfoliated structures where all the individual clay platelets have been effectively dispersed within the polymeric mass (the wide peak centered at 2Θ = 19.5° comes from the triblock copolymer). In Figure 1d, the pattern of the neat PS-*b*-PI-*b*-PS copolymer is given for comparison reasons.

In such nanocomposites, the enhanced dispersion of the clay nanolayers increases also the interaction of polymer with the CNTs rooted on the surface of the layers. On the other hand, PS-*b*-PI-*b*-PS nanocomposites with organoclay (C_{16}−SWy) as nanoadditive prepared with the same synthetic method and under the same experimental conditions showed a slightly different behavior (Figure 2).

The 001 reflection in the XRD patterns of C_{16}−SWy nanocomposites appeared at slightly higher 2θ angles compared to that of the parent powder organo-clay. The d_{001}-spacing for the PS-*b*-PI-*b*-PS nanocomposites prepared with 1 and 5 wt % C_{16}−SWy was found to be 17.7 and 16.8 Å, respectively, values which are slightly lower compared to the d_{001}-spacing of the

dx.doi.org/10.1021/jp309361b | J. Phys. Chem. B 2013, 117, 907−915

Scheme 2. Schematic Illustration of the Synthetic Steps Used for the Preparation of the PS-*b*-PI-*b*-PS−Clay−CNT Nanocomposites

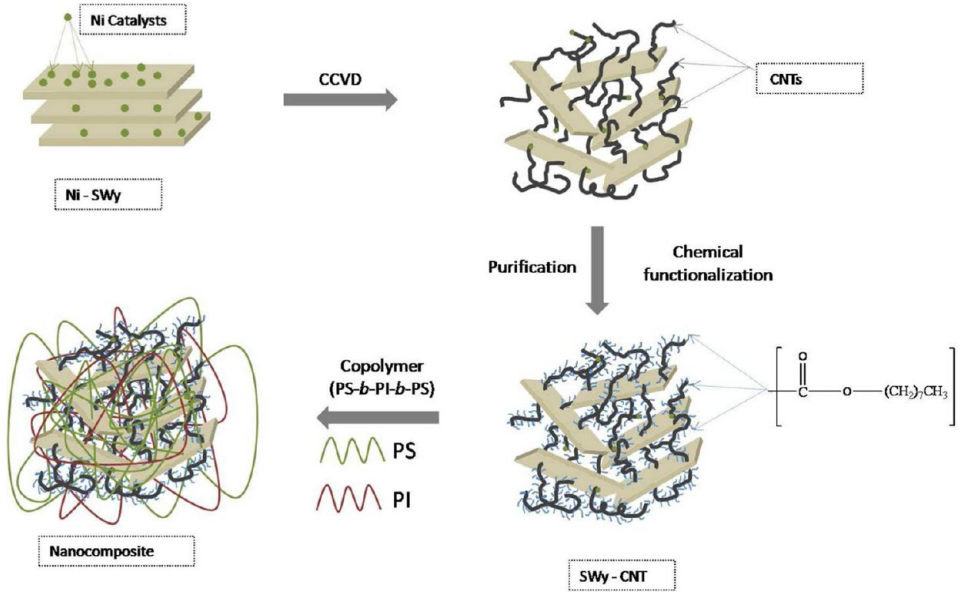

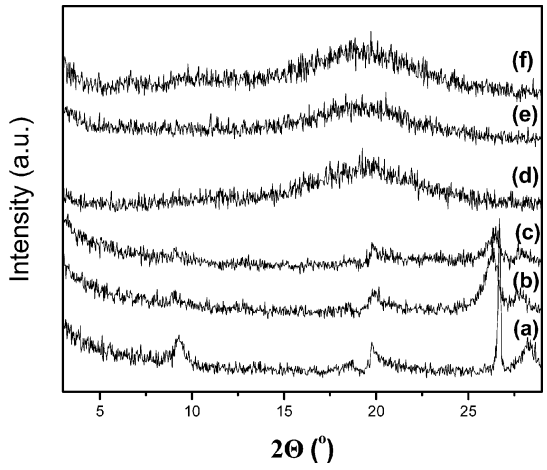

Figure 1. XRD patterns of Ni−SWy heated at 450 °C (a), SWy−CNTs before (b) and after (c) functionalization, neat PS-*b*-PI-*b*-PS copolymer (d), and final nanocomposites with 1 wt % (e) and 5 wt % (f) SWy−CNT.

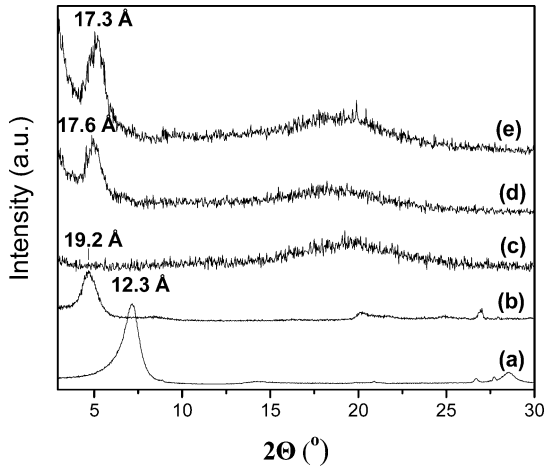

Figure 2. XRD patterns of (a) pristine Na−SWy, (b) organoclay C_{16}−SWy, (c) neat PS-*b*-PI-*b*-PS, and final nanocomposites loaded with (d) 1 wt % and (e) 5 wt % C_{16}−SWy.

organo-clay (18.8 Å). This decrease in the d_{001}-spacing may be attributed to rearrangement of the surfactant molecules within the galleries of the organo-clay upon removal of the water molecules during the preparation of the nanocomposites or to the insertion of a relatively small amount of polymer between the nanolayers. These structures can be characterized as microcomposites, since any possible reinforcement will actually derive from the organo-clay microparticles and not the individual clay nanolayers.

Raman spectroscopy is a valuable technique which can determine not only the quality of produced nanotubes and the degree of sidewall functionalization of CNTs but can also reveal the presence of nanotubes in the final polymer nanocomposites. Figure 3 shows the Raman spectrum of nanocomposite PS-*b*-PI-*b*-PI loaded with 5 wt % SWy−CNT in comparison with the spectra of neat polymer PS-*b*-PI-*b*-PS and the hybrid SWy−CNT nanoadditive before and after functionalization.

Two characteristic peaks at 1350 and 1595 cm^{-1} corresponding to graphite D- and G-bands, respectively, are observed in the Raman spectra of the clay−CNT nanoadditive before (Figure 3a) and after (Figure 3b) functionalizion of the CNTs. The G-band corresponds to the tangential stretching (E_{2g}) mode of highly oriented pyrolytic graphite (HOPG) and can be used to assess the degree of crystallinity/graphitisation, while the D-band at 1354 cm^{-1} originates from disorder in the sp^2-hybridized carbon atoms, characteristic of lattice distortions in the curved graphene sheets and/or tube ends.[32] The relative intensity of D- to G-bands (I_D/I_G) reveals the degree of disorder in the graphite sheets, and it can be used as a measure of the crystallinity and thus the quality of the synthesized CNTs.[33] The synthesized CNTs exhibit a very well graphitic structure as it is derived from the calculated values of the I_D/I_G ratios. In fact, the I_D/I_G ratio was calculated as 0.80 in the case of pristine clay−CNT nanoadditive, a value lower than those reported in the literature (I_D/I_G = 0.85−1.3) for CNTs prepared using acetylene as a carbon source.[34] After the

dx.doi.org/10.1021/jp309361b | J. Phys. Chem. B 2013, 117, 907−915

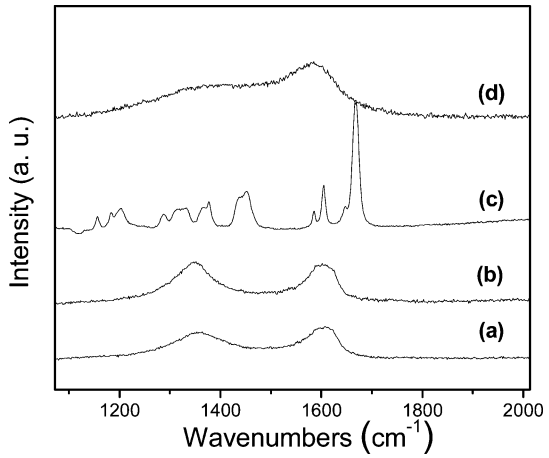

Figure 3. Raman spectra of SWy−CNTs before (a) and after (b) functionalization, neat PS-*b*-PI-*b*-PS copolymer (c), and nanocomposite with 5 wt % SWy−CNT (d).

chemical functionalization of the CNTs, the I_D/I_G ratio was increased to 1.03 due to the oxidation that was performed prior to the attachment of the aliphatic groups which induced structural changes in the nanotubes affecting the outer graphene layers. Finally, the two characteristic peaks of CNTs are also recorded at the spectrum of the final polymer nanocomposite (Figure 3d), indicating the presence of the hybrid nanoadditive in the final nanocomposite.

The presence of both the organo-clay and the clay−CNT hybrid nanoadditives in the final nanocomposites was revealed also with FTIR spectroscopy. Figure 4 (left) shows the FT-IR spectra of PS-*b*-PI-*b*-PS loaded with 5 wt % C_{16}−SWy in comparison with the spectra of the organoclay and the pristine triblock copolymer. The spectrum of the nanocomposite presents all the characteristic bands of the copolymer PS-*b*-PI-*b*-PS and of the organo-montmorillonite, without significant changes, confirming the presence of the organoclay in the final composite system. The appearance of the peaks at 465 and 1039 cm^{-1} which correspond to Si−O and Si−O−Si vibrations of the clay lattice[35] are indicative of the existence of the layered aluminosilicate mineral in the final composite. Similar, in the case of nanocomposite loaded with 5 wt % SWy−CNTs (Figure 4, right), the FTIR spectrum presents all the characteristic bands of the pristine copolymer plus the peak at 465 cm^{-1} which corresponds to Si−O vibration of the clay lattice, confirming the successful incorporation of the hybrid nanoadditive in the polymeric matrix.

Viscometry is a characterization technique employed in order to calculate the radius of gyration, which as we showed previously[23] leads to interesting results that verify the characterization results of the nanocomposites with the techniques described above. The best results in our previous work[23] occurred when the copolymer was in a 99:1 ratio with various low dimensional reinforcement materials when compared to the neat copolymer's value. The mean radius of gyration was minimized in the composite materials, a behavior which can be explained if one considers that the polymeric chains are being skewed when the nanostructured material is added, leading to a decrease in the distance from the periphery of the macromolecular entanglements. Using the Huggins and Kraemer equations, as shown below in relations 1 and 2, respectively, the plots of η_{sp}/C and $\ln \eta_r/C$ vs polymer concentration (C) can be obtained (η_{sp} and η_r correspond to the specific and the relative viscosity, respectively). From the mutual extrapolation to infinite dilution ($C \rightarrow 0$) of both equations, the intrinsic viscosity, $[\eta]$, can be calculated.

$$\eta_{sp}/C = [\eta] + K_H[\eta]^2 C \quad (1)$$

$$\ln \eta_r/C = [\eta] + K_C[\eta]^2 C \quad (2)$$

Finally, by using Flory's eq 3, the polymer's radius of gyration is calculated.

$$\langle \bar{S}^2 \rangle^{3/2} = \frac{[\eta] M_w}{\Phi} \quad (3)$$

$[\eta]$ is the intrinsic viscosity for the copolymer measured, $\bar{M}_w$ is the average molecular weight per weight of the triblock copolymer, and Φ is Flory's constant and equal to 2.5×10^{21} when $[\eta]$ is given in dL/g units and does not differ significantly for the two different segments. From the literature,[36] values for intrinsic viscosities and mean radius of gyration can be provided for both homopolymers (hPS and hPI, respectively). The results from the viscometry experiments are exhibited in Table S2 (Supporting Information). In Table S2, results are given for the intrinsic viscosity $[\eta]$ (in mL/g units) and the mean radius of gyration $\langle S^2 \rangle^{1/2}$ (in nm), respectively, by using the aforementioned relations for the neat copolymer, and for the

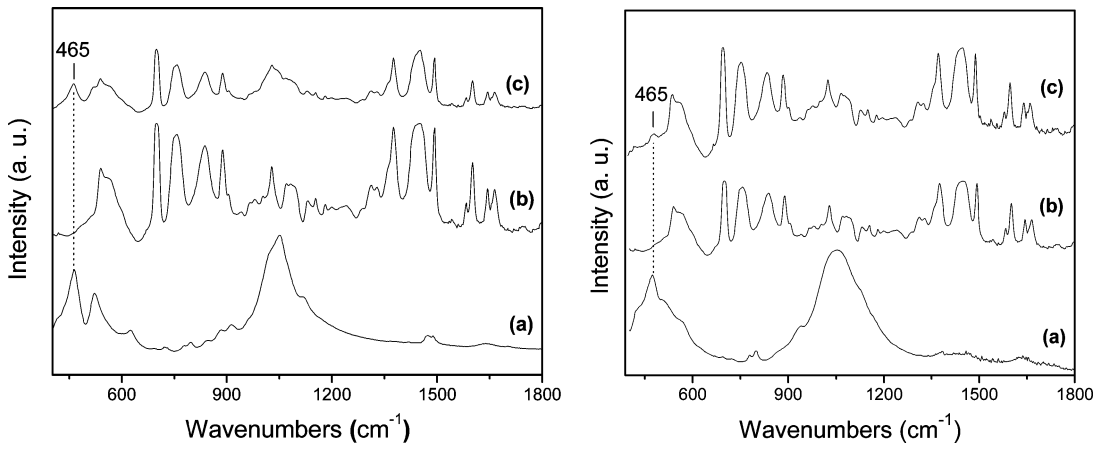

Figure 4. (left) FT-IR spectra of organoclay C_{16}−SWy (a), neat PS-*b*-PI-*b*-PS (b), and final nanocomposite with 5 wt % C_{16}−SWy (c). (right) FT-IR spectra of SWy−CNTs (a), neat PS-*b*-PI-*b*-PS copolymer (b), and final nanocomposites with 5 wt % SWy−CNT (c).

dx.doi.org/10.1021/jp309361b | J. Phys. Chem. B 2013, 117, 907−915

two composites of the copolymer with 1 wt % C_{16}−SWy and 1 wt % SWy−CNT, respectively. As in our previous work,[23] with just a simple diblock copolymer of the PS-*b*-PI type, we exhibit the same trend in the values of intrinsic viscosity when 1 wt % C_{16}−SWy and SWy−CNT are added in the triblock PS-*b*-PI-*b*-PS and the same behavior is exhibited as well for the radius of gyration values. In both cases, we observed a decrease in the intrinsic viscosity values which is much lower in the case of the organoclay nanoadditive (C_{16}−SWy). The differences are less distinct when compared with the diblock case[23] where enhanced intercalation of the polymer chains in the clay galleries is reported. This observation may be attributed to the fact that in the previous work (diblock PS-*b*-PI) both segments are end blocks, whereas in our case (PS-*b*-PI-*b*-PS) the PI chain is in the middle and is surrounded by two identical chains of PS not only in chemical structure but in molecular weight values as well. Additionally, the total molecular weight of the copolymer in the present study is much higher (132.1 kg/mol compared to 36.9 kg/mol in the diblock case). Therefore, the PI middle blocks are distributed in a much slower manner due to steric hindrance reasons. The very small changes in the radius of gyration for the two nanocomposites in the present study can be attributed to the fact that some of the polymer chains are distributed inside the interlayer space of the organophilic clay, therefore enhancing the flow and decreasing the flow time in the viscometer. The decrease is almost distinct in the case when SWy−CNT nanoadditives are being used. Therefore, the SWy−CNT hybrids are being distributed inside the polymer solution without affecting distinctively the viscometric properties of the copolymers, leading to well distributed hybrid nanostructured materials inside the entanglements of the polymeric chains.

TEM images give a clear morphological overview of the final nanocomposites revealing the presence of the nanoadditives within the polymer matrix. In the TEM image (Figure 5) of the PS-*b*-PI-*b*-PS nanocomposite loaded with 5 wt % clay−CNT nanoadditive (sample prepared through the dropcast technique), hollow carbon nanotubes can be easily observed within the bulk copolymer phase. In this case, no staining with vapors of OsO_4 was adopted in order to verify the copolymer, but instead we examined the sample unstained in order to better distinguish the CNTs. The average diameter (Figure 5, inset) of the carbon nanotubes is approximately 20 nm, while their length is of several micrometers.

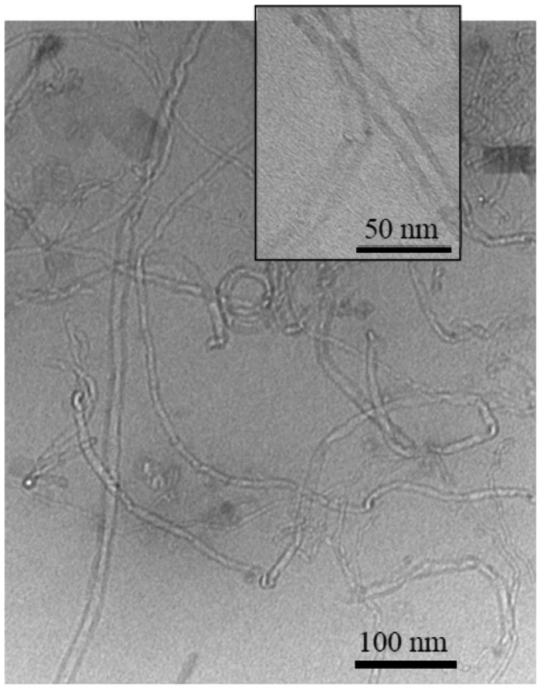

Figure 5. TEM images of the nanocomposite PS-*b*-PI-*b*-PS with 5 wt % SWy−CNT.

Although the CNTs were rooted on the surfaces of the layered mineral, it was difficult to observe the presence of the clay platelets directly linked to the clay nanolayers due to higher contrast of the CNTs when compared with the aluminosilicate nanoadditives. In the representative TEM image of the nanocomposite with 5 wt % C16−SWy organoclay (Figure 6), where OsO_4 was used to enhance the contrast of

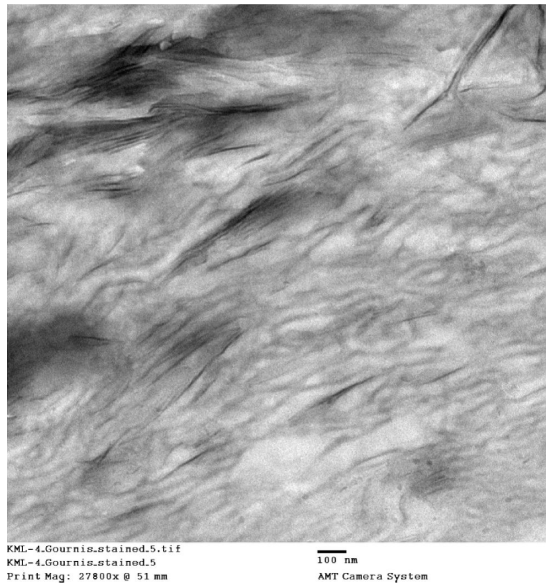

Figure 6. TEM image of nanocomposite PS-*b*-PI-*b*-PS with 5 wt % C_{16}−SWy.

the PI blocks of the copolymer, it can be seen that clay nanolayer tactoids (consisting of a small number of individual layers) are well dispersed within the bulk polymer. This can cause a significant alteration of the initial cylindrical morphology of the triblock copolymer.

This new structure is completely different, and microphase separation still occurs (white and gray to black regions) due to cross-linking of the PI blocks from the stainer. Therefore, in this case, the clay is not incorporated inside the polymer and therefore a bilayer system occurs with the clay on top and the polymer mass beneath it where the initial cylindrical structure of the copolymer remains.

The mechanical properties of the neat triblock copolymer and the respective nanocomposites were evaluated with tensile measurements, and the results are reported in Table 1.

More specifically, the average values of elastic modulus (E), tensile stress at yield (MPa), tensile stress at break (%), and tensile strain (elongation) at break (%) have been determined. In addition, the percentage (%) increase or decrease of the estimated parameters of the nanocomposites compared to those of the neat copolymer is also given in Table 1. The stress−strain curves (not shown for brevity) of all the samples

dx.doi.org/10.1021/jp309361b | J. Phys. Chem. B 2013, 117, 907−915

Table 1. Tensile Measurement Data for the PriStine Triblock Copolymer and the Nanocomposites with Organoclays and Hybrid Clay−CNT Nanoadditives[a]

sample	tensile stress at yield (MPa)	tensile stress at break (MPa)	tensile strain (elongation) at break (%)	elastic modulus (E, MPa)
neat PS-*b*-PI-*b*-PS	2.06 (0)	5.99 (0)	807 (0)	169 (0)
PS-*b*-PI-*b*-PS/1% C_{16}−SWy	2.32 (+13)	7.83 (+31)	894 (+11)	212 (+25)
PS-*b*-PI-*b*-PS/5% C_{16}−SWy	2.23 (+8)	4.19 (−30)	734 (−9)	225 (+33)
PS-*b*-PI-*b*-PS/1% SWy−CNTs	2.71 (+32)	10.5 (+75)	1010 (+25)	201 (+19)
PS-*b*-PI-*b*-PS/5% SWy−CNTs	2.85 (+38)	8.31 (+39)	1135 (+41)	255 (+51)

[a]The numbers in parentheses represent the % increase (positive values) or decrease (negative values) of the measured properties of the nanocomposites compared to the pristine polymer.

exhibited a clear transition from the elastic to plastic region (yield point) at relatively low and similar strain values (∼3−5%) for both the copolymer and the nanocomposites. On the other hand, the tensile stress values at yield point (Table 1) increased upon addition of organo-clay and hybrid clay−CNT nanoadditives, with the highest increase being induced by the hybrid materials (32−38%). It can thus be suggested that the presence of the hybrid clay−CNTs enhances the ability of the copolymer to adsorb larger amounts of mechanical stress. Accordingly, the elastic modulus (E) values of the nanocomposites were higher compared to the E value of the neat copolymer. The highest increase was observed for the nanocomposite with 5 wt % hybrid clay−CNT additive.

With regard to the tensile stress and strain at break (Table 1), addition of 1 wt % organoclay resulted in a considerable improvement of both parameters (31 and 11%, respectively), while a higher concentration of the organoclay (5 wt %) induced lower values compared to the neat copolymer. This could be attributed to the relatively high content of organoclay (compared to the 1 wt % addition) which is also accompanied with a larger amount of "dangling" C_{16}-alkylammonium chains of clay modifier. Both the high loading of organoclay (being probably in the intercalated state, as can be seen in Figure 2) as well as the C_{16}-hydrocarbon chains can disrupt the ordering of the copolymer crystalline structure and sacrifice the mechanical properties. On the other hand, in the case of the hybrid nanoadditives, the exfoliated state of clay nanolayers (Figure 1) in combination with the presence of carbon nanotubes grown on their surfaces, resulted in a significant improvement of both tensile stress and strain at break (Table 1). Functionalized CNTs rooted on smectite nanoclays seem to interact with the flexible rubbery PI chains in the copolymer matrix without thermodynamic penalties leading to enhanced mechanical properties. Such behavior cannot be accomplished by the glassy PS segments due to their decreased flexibility and increased steric hindrance. Further experiments on the rubbery-glassy-rubbery (PI-*b*-PS-*b*-PI) triblock copolymers are in progress in order to fully verify the important issue of enhanced mechanical properties for the rubbery phases when they are distributed as midblocks (SBR, SBS block copolymers which are already very well applied industrially).

4. CONCLUSIONS

In summary, novel nanocomposites of PS-*b*-PI-*b*-PS linear triblock copolymer with clay−CNT hybrid nanoadditives were prepared by a simple solution-precipitation method and compared with composites produced using typical organo-modified clay nanoadditives. The pristine triblock copolymer was synthesized via anionic polymerization techniques using sequential addition of the monomers in the solvent under high vacuum and characterized by SEC and ^{1}H NMR. In order to enhance the chemical compatibilization of the clay−CNT hybrid nanoadditives with the hydrophobic triblock copolymer, side-wall chemical organo-functionalization of the nanotubes was performed through covalent attachment of aliphatic groups on the surface of the nanotubes. XRD measurements confirmed the creation of fully exfoliated structures, while TEM images indicated that CNTs rooted on clay platelets were well dispersed within the polymer matrix. The presence of the hybrid nanoreinforcements in the final composite materials was also revealed through FT-IR and Raman measurements, while viscometry measurements showed that the SWy−CNT hybrids are being distributed inside the polymer solution without affecting distinctively the viscometric properties of the copolymers, leading to well distributed hybrid nanostructured materials inside the entanglements of the polymeric chains. Finally, tensile measurements showed that the exfoliated state of clay nanolayers in combination with the presence of carbon nanotubes grown on their surfaces resulted in significant improvement of both tensile stress and strain at break (stress at yield point and elastic modulus were also improved) of the copolymer by using the hybrid clay−CNT nanoadditives. This can be explained if we considered that the functionalized CNTs rooted on smectite nanoclays are in direct interaction with the flexible rubbery PI chains in the copolymer matrix leading to enhanced mechanical properties of the whole composite phase.

■ ASSOCIATED CONTENT

Supporting Information

Details on the anionic polymerization techniques used for the synthesis of the linear triblock copolymer are given together with results from size exclusion chromatography (Figure S1) and the molecular characteristics results (Table S1). Also included is Table S2 where the results from viscometry are given. This material is available free of charge via the Internet at http://pubs.acs.org.

■ AUTHOR INFORMATION

Corresponding Author

*E-mail: dgourni@cc.uoi.gr (D.G.); aavger@cc.uoi.gr (A.A.); ktrianta@chem.auth.gr (K.T.).

Author Contributions

The manuscript was written through contributions of all authors. All authors have given approval to the final version of the manuscript.

Notes

The authors declare no competing financial interest.

■ ACKNOWLEDGMENTS

The present work was supported in part by the "POCO" European Project (CP-IP213939-1) under the 7th Framework Program (FP7) and call NMP-2007-LARGE-1. The authors acknowledge cofunding of this research by the European Union—European Regional Development Fund and the Greek

Ministry of Education/EYDE-ETAK through program ESPA 2007-2013/EPAN II/Action "SYNERGASIA" (project 09SYN-42-831). The authors would like to acknowledge the use of the XRD unit and the NMR Facility of the Laboratory Network, at the University of Ioannina.

REFERENCES

(1) Tseng, Y. C.; Darling, S. B. *Polymers* **2010**, *2*, 470−489.
(2) Bates, F. S.; Fredrickson, G. H. *Phys. Today* **1999**, *52*, 32−38.
(3) (a) Quirk, R. P.; Morton, M. In *Thermoplastic Elastomers*; Hanser Publishers: New York, 1996; pp 77−100. (b) Honeker, C. C.; Thomas, E. L. *Chem. Mater.* **1996**, *8*, 1702−1714.
(4) (a) Dair, B. J.; Honeker, C. C.; Alward, D. B.; Avgeropoulos, A.; Hadjichristidis, N.; Fetters, L. J.; Capel, M.; Thomas, E. L. *Macromolecules* **1999**, *32*, 8145−8152. (b) Dair, B. J.; Avgeropoulos, A.; Hadjichristidis, N.; Thomas, E. L. *J. Mater. Sci.* **2000**, *35*, 5207−5213. (c) Dair, B. J.; Avgeropoulos, A.; Hadjichristidis, N.; Capel, M.; Thomas, E. L. *Polymer* **2000**, *41*, 6231−6236.
(5) Avgeropoulos, A.; Dair, B. J.; Hadjichristidis, N.; Thomas, E. L. *Macromolecules* **1997**, *30*, 5634−5642.
(6) (a) Kojima, Y.; Usuki, A.; Kawasumi, M.; Okada, A.; Kurauchi, T.; Kamigaito, O. *J. Polym. Sci., Part A: Polym. Chem.* **1993**, *31*, 983−986. (b) Sinha Ray, S.; Okamoto, M. *Prog. Polym. Sci.* **2003**, *28*, 1539−1641.
(7) (a) Giannelis, E. P. *Adv. Mater.* **1996**, *8*, 29−35. (b) Leroux, F.; Besse, J. P. *Chem. Mater.* **2001**, *13*, 3507−3515. (c) Paul, D. R.; Robeson, L. M. *Polymer* **2008**, *49*, 3187−3204. (d) Rahman, A.; Ali, I.; Al Zahrani, S. M.; Eleithy, R. H. *Nano* **2011**, *6*, 185−203.
(8) (a) Jacob, M. M. E.; Hackett, E.; Giannelis, E. P. *J. Mater. Chem.* **2003**, *13*, 1−5. (b) Gournis, D.; Floudas, G. *Chem. Mater.* **2004**, *16*, 1686−1692. (c) Xidas, P. I.; Triantafyllidis, K. S. *Eur. Polym. J.* **2010**, *46*, 404−417.
(9) Blumstein, A. *J. Polym. Sci., Part A* **1965**, *3*, 2665−2672.
(10) (a) Kojima, Y, U. A.; Kawasumi, M.; Okada, A.; Kurauchi, T.; Kamigaito, O. *J. Polym. Sci., Part A: Polym. Chem.* **1993**, *31*, 1755−1758. (b) Sinha Ray, S.; Yamada, K.; Okamoto, M.; Ueda, K. *Polymer* **2003**, *44*, 857−866.
(11) Triantafyllidis, K. S.; LeBaron, P. C.; Park, I.; Pinnavaia, T. J. *Chem. Mater.* **2006**, *18*, 4393−4398.
(12) Triantafyllidis, K. S.; LeBaron, P. C.; Pinnavaia, T. J. *J. Solid State Chem.* **2002**, *167*, 354−362.
(13) Pinnavaia, T. J., Beall, G. W., Eds. *Polymer-Clay Nanocomposites*; J. Wiley & Sons: New York, 2001.
(14) Iijima, S. *Nature* **1991**, *354*, 56−58.
(15) (a) Baughman, R. H.; Zakhidov, A. A.; De Heer, W. A. *Science* **2002**, *297*, 787−792. (b) Ajayan, P. M. *Chem. Rev.* **1999**, *99*, 1787−1799.
(16) (a) Li, Y. L.; Kinloch, I. A.; Windle, A. H. *Science* **2004**, *304*, 276−278. (b) Dalton, A. B.; Collins, S.; Muñoz, E.; Razal, J. M.; Ebron, V. H.; Ferraris, J. P.; Coleman, J. N.; Kim, B. G.; Baughman, R. H. *Nature* **2003**, *423*, 703.
(17) Qian, D.; Dickey, E. C.; Andrews, R.; Rantell, T. *Appl. Phys. Lett.* **2000**, *76*, 2868−2870.
(18) (a) Li, S.; Qin, Y.; Shi, J.; Guo, Z. X.; Li, Y.; Zhu, D. *Chem. Mater.* **2005**, *17*, 130−135. (b) Lin, Y.; Zhou, B.; Fernando, K. A. S.; Liu, P.; Allard, L. F.; Sun, Y. P. *Macromolecules* **2003**, *36*, 7199−7204. (c) Viswanathan, G.; Chakrapani, N.; Yang, H.; Wei, B.; Chung, H.; Cho, K.; Ryu, C. Y.; Ajayan, P. M. *J. Am. Chem. Soc.* **2003**, *125*, 9258−9259. (d) Qin, S.; Qin, D.; Ford, W. T.; Resasco, D. E.; Herrera, J. E. *J. Am. Chem. Soc.* **2004**, *126*, 170−176. (e) Zhang, W. D.; Shen, L.; Phang, I. Y.; Liu, T. *Macromolecules* **2004**, *37*, 256−259.
(19) Gournis, D.; Karakassides, M. A.; Bakas, T.; Boukos, N.; Petridis, D. *Carbon* **2002**, *40*, 2641−2646.
(20) Zhang, W. D.; Phang, I. Y.; Liu, T. *Adv. Mater.* **2006**, *18*, 73−77.
(21) Zhao, Y. Q.; Lau, K. T.; Wang, Z.; Wang, Z. C.; Cheung, H. Y.; Yang, Z.; Li, H. L. *Polym. Compos.* **2009**, *30*, 702−707.
(22) Wang, Z.; Xu, C.; Zhao, Y.; Zhao, D.; Wang, Z.; Li, H.; Lau, K. T. *Mater. Sci. Eng., A* **2008**, *490*, 481−487.
(23) Litina, K.; Miriouni, A.; Gournis, D.; Karakassides, M. A.; Georgiou, N.; Klontzas, E.; Ntoukas, E.; Avgeropoulos, A. *Eur. Polym. J.* **2006**, *42*, 2098−2107.
(24) (a) Hsu, H. L.; Jehng, J. M. *Mater. Sci. Eng., C* **2009**, *29*, 55−61. (b) Hsu, H. L.; Jehng, J. M.; Liu, Y. C. *Mater. Chem. Phys.* **2009**, *113*, 166−171.
(25) (a) Avgeropoulos, A.; Chan, V. Z. H.; Lee, V. Y.; Ngo, D.; Miller, R. D.; Hadjichristidis, N.; Thomas, E. L. *Chem. Mater.* **1998**, *10*, 2109−2115. (b) Chan, V. Z. H.; Hoffman, J.; Lee, V. Y.; Iatrou, H.; Avgeropoulos, A.; Hadjichristidis, N.; Miller, R. D.; Thomas, E. L. *Science* **1999**, *286*, 1716−1719.
(26) (a) Avgeropoulos, A.; Hadjichristidis, N. *J. Polym. Sci., Part A: Polym. Chem.* **1997**, *35*, 813−816. (b) Hadjichristidis, N.; Tselikas, Y.; I., H.; Efstratiadis, V.; Avgeropoylos, A. *J. Macromol. Sci, Part A: Pure Appl. Chem.* **1996**, *A 33*, 1447.
(27) Gournis, D.; Lappas, A.; Karakassides, M. A.; Tobbens, D.; Moukarika, A. *Phys. Chem. Miner.* **2008**, *35*, 49−58.
(28) Jankovic, L.; Gournis, D.; Dimos, K.; Karakassides, M. A.; Bakas, T. *J. Phys.: Conf. Ser.* **2005**, *10*, 178−181.
(29) Tsoufis, T.; Jankovic, L.; Gournis, D.; Trikalitis, P. N.; Bakas, T. *Mater. Sci. Eng., B* **2008**, *152*, 44−49.
(30) Newman, A. C. D. *Chemistry of Clays and Clay Minerals*; Mineralogical Society Monograph, No. 6; Longman: London, 1987.
(31) Zhu, W. Z.; Miser, D. E.; Chan, W. G.; Hajaligol, M. R. *Mater. Chem. Phys.* **2003**, *82*, 638−647.
(32) (a) Furtado, C. A.; Kim, U. J.; Gutierrez, H. R.; Pan, L.; Dickey, E. C.; Eklund, P. C. *J. Am. Chem. Soc.* **2004**, *126*, 6095−6105. (b) Li, W. Z.; Zhang, H.; Wang, C. Y.; Zhang, Y.; Xu, L. W.; Zhu, K.; Xie, S. S. *Appl. Phys. Lett.* **1997**, *70*, 2684−2686. (c) Georgakilas, V.; Gournis, D.; Karakassides, M. A.; Bakandritsos, A.; Petridis, D. *Carbon* **2004**, *42*, 865−870.
(33) (a) Maccallini, E.; Tsoufis, T.; Policicchio, A.; La Rosa, S.; Caruso, T.; Chiarello, G.; Colavita, E.; Formoso, V.; Gournis, D.; Agostino, R. G. *Carbon* **2010**, *48*, 3434−3445. (b) Tsoufis, T.; Xidas, P.; Jankovic, L.; Gournis, D.; Saranti, A.; Bakas, T.; Karakassides, M. A. *Diamond Relat. Mater.* **2007**, *16*, 155−160.
(34) (a) Sveningsson, M.; Morjan, R. E.; Nerushev, O. A.; Sato, Y.; Backstrom, J.; Campbell, E. E. B.; Rohmund, F. *Appl. Phys. A: Mater. Sci. Process.* **2001**, *73*, 409−418. (b) Dresselhaus, M. S.; Dresselhaus, G.; Jorio, A.; Souza Filho, A. G.; Saito, R. *Carbon* **2002**, *40*, 2043−2061.
(35) (a) Karakassides, M. A.; Petridis, D.; Gournis, D. *Clays Clay Miner.* **1997**, *45*, 649−658. (b) Karakassides, M. A.; Gournis, D.; Petridis, D. *Clay Miner.* **1999**, *34*, 429−438.
(36) (a) Pispas, S.; Avgeropoulos, A.; Hadjichristidis, N.; Roovers, J. *J. Polym. Sci., Part B: Polym. Phys.* **1999**, *37*, 1329−1335. (b) Prudhomm, J.; Bywater, S.; Roovers, J. E. L. *Eur. Polym. J.* **1972**, *8*, 901−910. (c) Roovers, J. E. L.; Bywater, S. *Macromolecules* **1972**, *5*, 384−388. (d) Hadjichristidis, N.; Roovers, J. E. L. *J. Polym. Sci., Part B: Polym. Phys.* **1974**, *12*, 2521−2533.